Available online at www.sciencedirect.com
ScienceDirect
Materials Research Bulletin 41 (2006) 1604–1611
Materials Research Bulletin
www.elsevier.com/locate/matresbu

Effect of the surface configuration on the oxidation of bismuth nanowire

C.C. Huang *, K.Z. Fung

Department of Materials Science and Engineering, National Cheng Kung University, Tainan 70101, Taiwan

Received 1 September 2005; received in revised form 11 January 2006; accepted 21 February 2006
Available online 29 March 2006

Abstract

Incorporating nanoprocessing into the metal oxidation, it was a facile way to synthesize functional oxide with desired nanostructure. In this work, δ-Bi_2O_3 nanowires were successfully fabricated by the oxidation of electroplated Bi nanowires at 350 °C. δ-Bi_2O_3 is the high-temperature phase of Bi_2O_3 and only stable at 723–823 °C. Partially oxidized nanowires showed core-shell structure composed of metallic Bi and δ-Bi_2O_3. To investigate the mechanism of oxidation reaction, the Bi/Bi_2O_3 interface was characterized by high resolution transmission electron microscopy (HRTEM). HRTEM images showed rapid growth of oxide layer on $(2\bar{1}0)$ plane of rhombohedral Bi metal. The coherency between $(10\bar{2})$ of metallic Bi and (1 0 0) of cubic Bi_2O_3 was observed. A schematic model was also used to describe the oxidation process. The coherency Bi and Bi_2O_3 and the stabilization of high-temperature (fluorite structure) Bi_2O_3 were also discussed based on this model.

Keywords: Metal; Oxidation; Crystal growth

1. Introduction

Bismuth oxide (Bi_2O_3) thin films are of significantly wide band gap, high refractive index, dielectric permittivity, photoconductivity, and photoluminescence [1–6]. Therefore, Bi_2O_3 can be used for optical coatings, Schottky barrier solar cell and metal/insulator/semiconductor (MIS) capacitors [2,7,8]. In addition, fluorite-structured δ-Bi_2O_3 exhibits the highest oxygen ionic conductivity that is desired (1 S/cm at 800 °C) for high-temperature electrochemical application such as SOFC and oxygen pump [9]. The rapid ionic conduction of δ-Bi_2O_3 was due to the fluorite structure with 25% anionic vacancies. Hence, δ-Bi_2O_3 has the favored structure to be used as a solid electrolyte. Owing to its defective structure, the δ-Bi_2O_3 is only stable at 723–823 °C [10]. However, δ-phase can be stabilized by adding rare earth oxides [11–16]. In addition to doped-Bi_2O_3 prepared by solid state syntheses, thin films with polycrystalline bismuth oxide were also prepared by thermal evaporation [17], thermal oxidation [6,18], activated reactive evaporation [19], chemical spray pyrolysis [20], and chemical vapor deposition [21], pulsed laser deposition [22]. Switzer et al. and Takeyama et al. also pointed out novel methods for preparing single crystalline δ-Bi_2O_3 by electroplating [23,24] and halide chemical vapour deposition (AP-HCVD) [25], respectively.

For electrochemical applications, a nanostructure established at the electrode/electrolyte interface would increase the triple phase boundary (TPB) and then minimize the activation polarization causing the degradation of voltage.

* Corresponding author. Tel.: +886 6 2757575x62969; fax: +886 6 2380208.
E-mail address: sceruti@mse.ncku.edu.tw (C.C. Huang).

0025-5408/$ – see front matter © 2006 Elsevier Ltd. All rights reserved.
doi:10.1016/j.materresbull.2006.02.037

Anodic alumina oxide (AAO) template-assisted method provides a facile way to prepare metal nanowires [26,27]. Based on the Leontie's research, bismuth oxide can be prepared by oxidation of Bi under controlled condition and revealed significant optical properties [5,6,18]. In this work, core-shelled Bi/δ-Bi_2O_3 composite nanowires were prepared by the similar method to investigate the mechanism of the structural relationship between metal and oxide. The coherent relationship between rhombohedral Bi and cubic δ-Bi_2O_3 was studied by HRTEM and select area electron diffraction (SAED). As we know, δ-Bi_2O_3 is not the thermodynamically equilibrium phase at temperature $<$723 °C. Thus, the stabilization of this high-temperature phase without the presence of dopants is unusual and worth of further investigation.

2. Experimental procedure

2.1. Preparation of Bi nanowires

An Al sheet (99.997% purity; Alfa aluminum foil; Johnson Matthey, Ward Hill, MA) of 1 mm thick was used as the starting material for anodization. After a common process for AAO fabrication, large area nanopores with 47 nm in average diameter were obtained. A Pt layer of 20 nm thick was deposited on the backside of the porous alumina as the cathode. Bi nanowires were fabricated by electroplating method. The deposited Pt layer was served as the working electrode in a conventional three-electrode cell for electrodeposition using potentiostat/galvanostat meter (EG&G 263 A). Graphite plate was used as the counter electrode. The electrolyte solution was composed of 48.57 g $Bi(NO_3)_3{\cdot}5H_2O$, 700 ml ethylene glycol and 300 ml distilled water. To ensure a stable electrodeposition process, the solution was stirred for 24 h to dismiss the additional bubbles. The reference electrode was soaked in a separate beaker with a saturated NaCl solution and connected to deposition bath by a NaCl/Pt salt bridge. Owing to the neutral solution, the AAO template would not be dissolved during deposition process and remained its nanoporous morphology. Subsequently, a voltage of −0.15 V versus Ag/AgCl reference electrode was applied for 10 h to overfill the AAO template with Bi. After the overfilling, the film was rinsed by distilled water, as-deposited samples were then pasted on a solid substrate (Au coated Si wafer) by Ag adhesive. The specimen was bathed in 3 M aqueous NaOH for 2 h to dissolve the AAO template. To separate the residual solution, the samples were also immersed in water for 30 min and rinsed with distilled water several times. The morphology of Bi nanowires was examined using scanning electron microscope (SEM, Hitachi S4100). Transmission electron microscope (TEM, JEOL-3010) and electron diffraction (ED) were used for structural analysis of single nanowire.

2.2. Oxidation of Bi nanowires

The specimen was annealed at 250 °C to obtain a partially oxidized or core-shell nanowire. To collect the nanowires for TEM analysis, the nanowires were scraped off and dispersed in ethanol. Then, several drops of alcohol were put on the 325 mesh copper grid. Transmission electron microscope (TEM, JEOL-3010) and electron diffraction (ED) attached to HRTEM were used for structural analysis of single nanowire.

3. Results and discussion

3.1. Fabrication of Bi/δ-Bi_2O_3 core-shell nanowire

In our previous work, δ-Bi_2O_3 nanowires were obtained after full oxidation process at 350 °C [28]. For the investigation of the metal/oxide interface, Bi and δ-Bi_2O_3 coexisting core-shell structure nanowires were also prepared at 250 °C in this work. From the TEM results shown in Fig. 1(a), the Bi nanowire annealed at 250 °C for 5 h was covered with an oxide layer. According to the SAED pattern along [0 0 1] axis of rhombohedral Bi shown in Fig. 1(b), the center of nanowires remained to be metallic Bi with the rhombohedral structure. However, several diffraction rings were also observed from the pattern. Obviously, the *d*-spaces of these rings did not match with that of any plane in the rhombohedral Bi. Fig. 1(c) showed the SAED patterns of the outer layer, which is consistent with the pattern along [0 0 1] zone axis of cubic δ-Bi_2O_3. In this pattern, diffraction rings similar to those in Fig. 2(b) were also observed. Subsequently, these rings were attributed to families of (0 0 2) and (0 0 4) of cubic δ-Bi_2O_3 by considering the

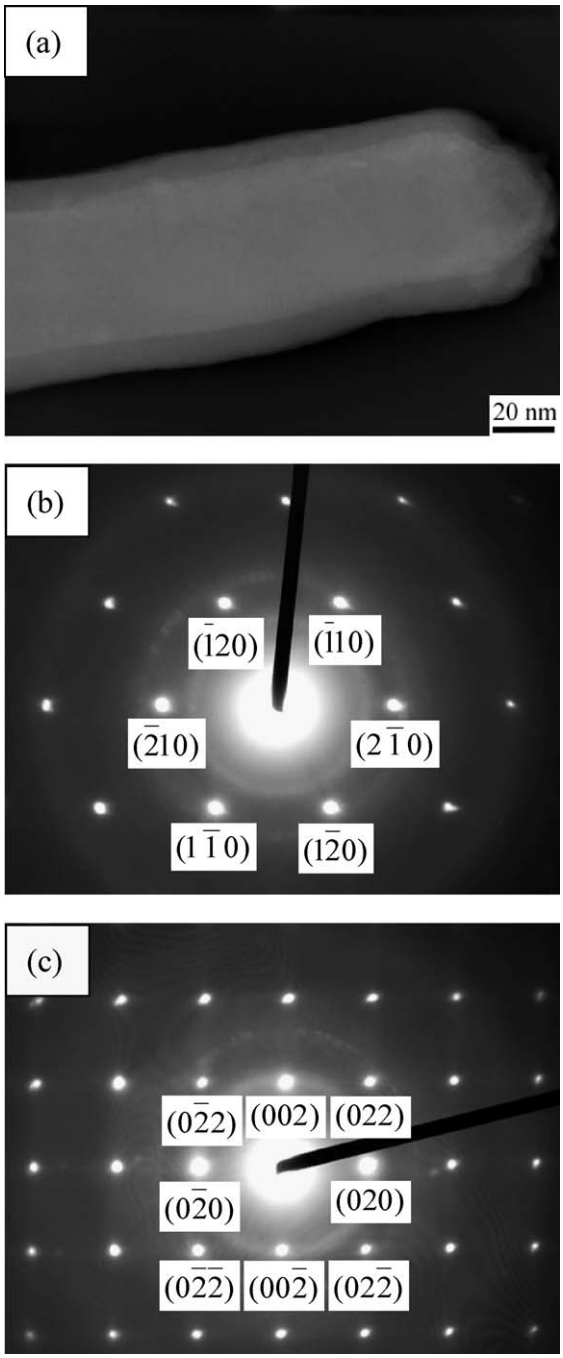

Fig. 1. (a) TEM image of a core-shell nanowire, (b) SAED pattern of central wire and (c) SAED pattern of outer layer.

corresponding of *d*-spacings. The results pointed out that the core-shell structure was composed of the metallic Bi and covered with fine-grained δ-Bi_2O_3.

3.2. HRTEM analyses of Bi/δ-Bi_2O_3 interface

In order to examine the lattice relationship between rhombohedral Bi and cubic δ-Bi_2O_3, high resolution TEM was employed to study the corresponding lattice image and related diffraction patterns. Since the oxidation reaction

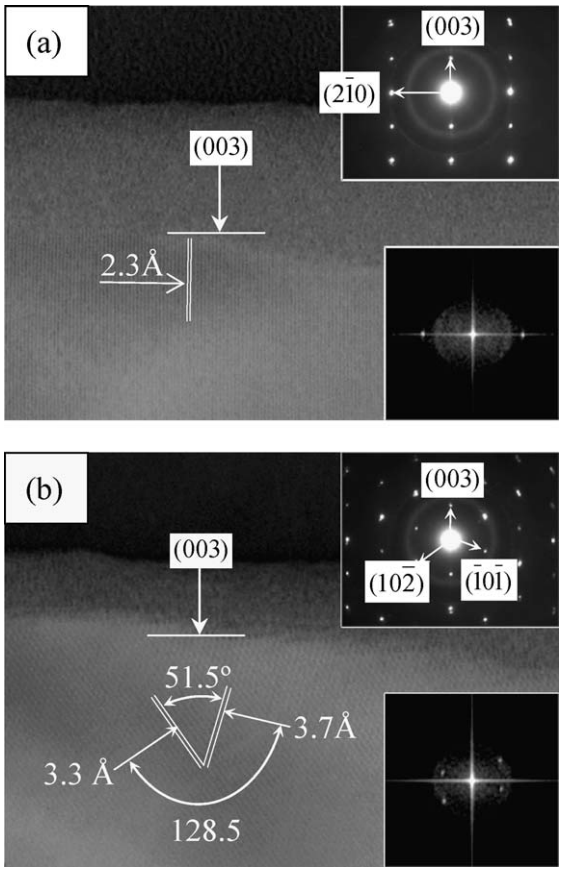

Fig. 2. HRTEM images and SAED patterns along (a) [1 2 0] and (b) [0 1 0] zone axis.

usually requires diffusion of metal or oxygen ions through the oxide layer, the most important mechanism of metal oxidation is the complex interaction at metal surface [29]. From the prior works, the phases of bismuth oxide layer can also be controlled by the prefer orientations of the metallic thin film [30]. Accordingly, the surface configuration of the metal/oxide interface was also examined using high resolution transmission electron microscopy (HRTEM) as shown in Fig. 2. Again, the central wire and outer layer belong to rhombohedral Bi and cubic δ-Bi_2O_3, respectively. In Fig. 2(a), distinct lattice lines perpendicular to the interface were observed. To identify the plane corresponding to these lattice images, both the measurement of the *d*-spacing and the relative SAED pattern were carefully analyzed. The measured *d*-spacing from the lattice lines was 2.3 Å representing the $(2\bar{1}0)$ plane (2.273 Å) of rhombohedral Bi. Based on the relationship of real and reciprocal lattice, the crystal structure was characterized by the Fourier transformation and the SAED pattern as shown in the insets. From the Fourier transformation of the lattice image, the transformed points shown in the inset also matched the SAED pattern. Since the SAED pattern was found to be along [1 2 0] zone axis, the corresponding diffraction planes were indexed. As shown in Fig. 2(b), two lattice lines which were of different *d*-spacings, 3.3 and 3.7 Å, respectively, and an angel of 51.5° were observed. Correspondingly, the planes were characterized to be $(10\bar{2})$ and $(\bar{1}0\bar{1})$. From the perpendicular relationship of *d*- and *R*-spacing, the observed angle matched theoretical plane angle (128.05°) as shown in the diffraction pattern. By the characterizing the SAED patterns and HR images, the real structure and orientations of the planes can also be examined. Hence, the observed Bi/δ-Bi_2O_3 interface is (0 0 3) as the reflections shown in Fig. 2.

3.3. Favored orientation of Bi for the formation of δ-Bi_2O_3

After annealing at 250 °C for 24 h, a very distinct core-shell structure was obtained as shown in Fig. 3(a). Obviously, most of this nanowire was oxidized except the central cylinder. From the DF image, the oxidized nanowire

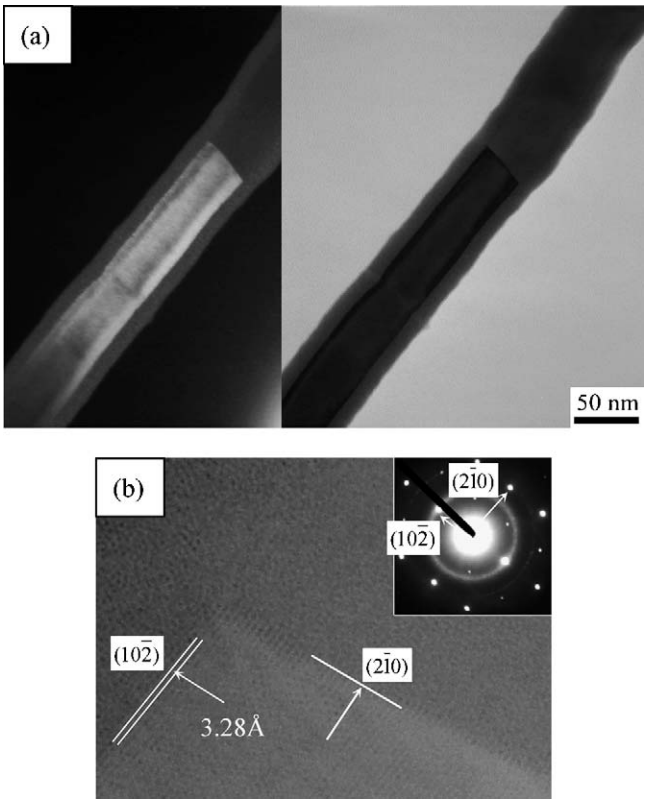

Fig. 3. (a) BF and DF images and (b) HRTEM image and SEAED pattern of the core-shell nanowire.

showed two different phases of Bi and δ-Bi_2O_3. In order to examine the interface of Bi and δ-Bi_2O_3, HRTEM and SAED pattern were also used. From Fig. 3(b), the HR image near the interface clearly shows the lattice line of Bi metal. The *d*-spacing was measured to be 3.28 Å that corresponds to the $(10\bar{2})$ lateral plane of Bi metal. According to the diffraction pattern in Fig. 3(b), the Bi plane facing the axial direction would be the $(2\bar{1}0)$ plane although the lattice image was not clearly observed. In Fig. 3(a), the oxide layer growing in the direction normal to $(10\bar{2})$ plane exhibits a thickness of 13.7 nm. In addition, the oxide layer growing in the direction normal to $(2\bar{1}0)$ plane are much thicker than that normal to $(10\bar{2})$ plane. Consequently, TEM analyses including SAED patterns and HR images indicated the (0 0 3), $(10\bar{2})$ and $(2\bar{1}0)$ interfaces. However, the $(2\bar{1}0)$ plane exhibits significant rapid oxidation rate than others. Such difference was analyzed based on lattice relationship between Bi and Bi_2O_3 as what follows.

3.4. Lattice relationship between rhombohedral Bi and cubic δ-Bi_2O_3

A theoretical crystal structure of Bi with space group of $R\bar{3}m$ is shown in Fig. 4(a). The lattice parameter of rhombohedral Bi was $a = b = 0.455$ nm $\neq c = 1.187$ nm and $\alpha = \beta = 90^\circ \neq \gamma = 120^\circ$. As the arrangement of Bi atom was drawn based on the hexagonal symmetry. In Fig. 4(a), a monoclinic or pseudo-tetragonal subcell was selected in the rhombohedral Bi lattice with the parameters, $a = 0.455$ nm, $b = 0.474$ nm, $c = 0.657$ nm, $\alpha = 93.37^\circ$, $\beta = 90.03^\circ$, and $\gamma = 90^\circ$. To associate with the subcell, the $(2\bar{1}0)$ plane of rhombohedral matched well with the (1 0 0) plane of the pseudo-tetragonal lattice. It is deserved to be mentioned that the $(2\bar{1}0)$ was also the fast-growing plane of the Bi/δ-Bi_2O_3 interface. Hence, the mechanism of Bi oxidation may be viewed from Fig. 5. At first, the Bi lattice exhibits about 48.8% open space. The oxygen may diffuse through the $(2\bar{1}0)$ because this plane provide opening of 1.39 Å for the migration of oxygen. Subsequently, the Bi atom in center layer migrate 1/2 of unit length in the direction perpendicular to $(2\bar{1}0)$ in order to eight-fold coordination with oxygen. After oxidation, larger Bi atom (1.68 Å) transformed three electrons to oxygen and became Bi^{3+} ion with smaller ionic radius of 1.17 Å. With the migration of Bi ions and formation of Bi–O bonding, the pseudo-tetragonal lattice slightly expands to cubic lattice. The cell volume also

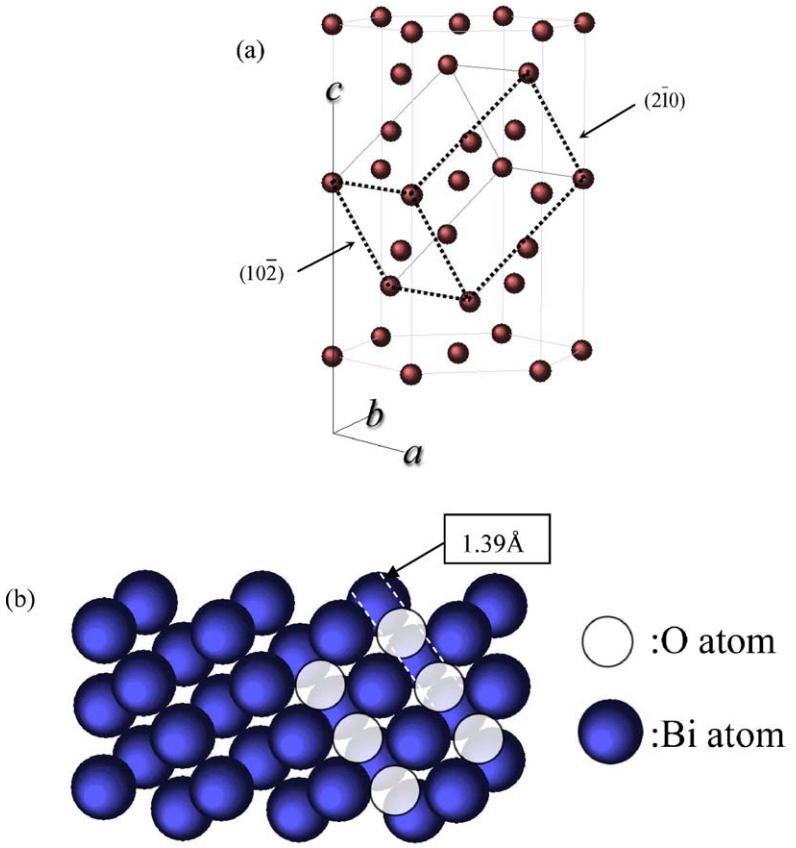

Fig. 4. (a) crystal structure of rhombohedral Bi and (b) atomic configuration of $(2\bar{1}0)$ plane in rhombohedral Bi lattice.

changes from 128.89 to 162.77 $Å^3$. In addition, the diffusion of oxygen is much easier in the direction perpendicular to $(2\bar{1}0)$ plane. Thus, the oxide tends to grow in the direction normal to $(2\bar{1}0)$ plane. From the observation of TEM micrograph, the oxidation rate along the lateral direction (normal to $(2\bar{1}0)$) is significantly higher than that along side way of the Bi nanowire. More importantly, due to the similarity between the monoclinic lattice (or pseudo-tetragonal) of Bi and the cubic lattice of Bi_2O_3, minimum of structure destruction/distortion is needed. Combining the results of faster growth in the direction perpendicular to $(2\bar{1}0)$ and the atomic arrangement of Bi in a rhombohedral lattice, an oxidation process was proposed through the atom rearrangement shown in Fig. 4(b). Owing to larger free space (1.39 Å) on $(2\bar{1}0)$, oxygen molecules dissociate, ionize and migrate into pseudo-tetragonal during the oxidation

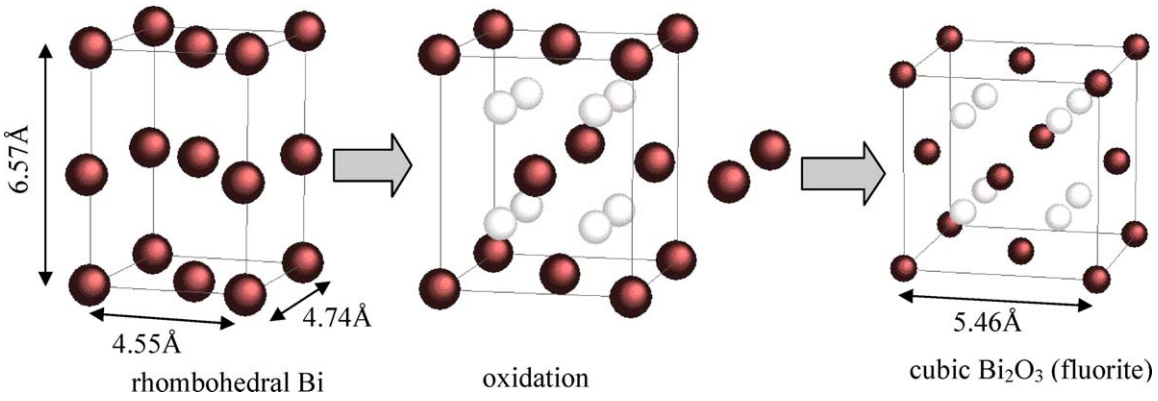

Fig. 5. Structural schematic diagram of phase transformation from rhombohedral Bi to cubic Bi_2O_3.

reaction. Subsequently, the formation of ionic bonding results the half unit translation of Bi planes. Eight oxygen ions were able to incorporate into the pseudo-tetragonal lattice. Due to the larger ionic radius of oxygen, the axis was expanded from 4.54 to 5.46 Å. On the other hand, the strong ionic bondings also bring oxygen ion and Bi ion closer along the c-axis direction. Consequently, a cubic fluorite lattice was obtained. Such a geometric and atomic movement consideration shows very good agreement with the faster growth of Bi_2O_3 in the direction normal to $(2\bar{1}0)$. After the oxidation, the cell volume expanded from 128.89 to 162.77 $Å^3$. The minimal atomic movement and limited volume expansion is the main reason for the relatively fast oxidation.

3.5. Formation of δ-Bi_2O_3 with high-temperature defective structure

From the SAED pattern shown in Fig. 1(c), the oxide layer exhibits cubic structure and belongs to δ-Bi_2O_3. As we know that the thermodynamically equilibrium phase of Bi_2O_3 should be α-Bi_2O_3 with monoclinic structure. The phase transformation of δ → α-Bi_2O_3 phase is basically caused by the very defective fluorite structure of Bi_2O_3 in which 25% of anion sites are vacant. Thus, α-Bi_2O_3 is constructed of layer by layer arrangement of B^{3+} and O^{2-} without the presence of oxygen vacancies. However, based on previous TEM results, the oxidation of Bi nanowires surprisingly formed the metastable δ-Bi_2O_3 phase that is only stable at temperatures >723 °C [28]. From the Bi/Bi_2O_3 interface observed, the atomic arrangement or lattice relationship should play an important role on the stabilization of δ-Bi_2O_3 at temperature as low as 250 °C. From previous discussion, the formation of cubic δ-Bi_2O_3 is favored due to the limited migration of Bi and large free space for the migration of oxygen. In addition, the cubic δ-Bi_2O_3 with 25% anion site vacant is known to be an excellent oxygen ion conductor. Thus, the rapid migration of oxygen ion also enhances the growth of cubic δ-Bi_2O_3. Therefore, when Bi nanowires were oxidized at temperatures as low as 250–350 °C, the nucleation and growth of δ-Bi_2O_3 is favored.

4. Conclusions

It was observed that the $(2\bar{1}0)$ plane of Bi was found to be coherent with the fast-growing (1 0 0) plane of δ-Bi_2O_3 during the oxidation process. Based on the results of HRTEM and SAED, a schematic model through the oxidation of Bi nanowires was illustrated. By converting the rhombohedral structure to pseudo-tetragonal subcell, the $(2\bar{1}0)$ plane provides the larger free space for oxygen ions to migrate. The limited transformation of Bi atoms during the oxidation favors the formation of high-temperature phase, δ-Bi_2O_3.

Acknowledgement

This research was supported by the National Science Council, Grant No. NSC 94-2120-M-006-002.

References

[1] P.B. Clapham, Br. J. Appl. Phys. 18 (1967) 363.
[2] H. Gobrecht, S. Seeck, H.-E. Bergt, A. Märtens, K. Kossmann, Phys. Stat. Sol. 33 (1969) 599; H. Gobrecht, S. Seeck, H.-E. Bergt, A. Märtens, K. Kossmann, Phys. Stat. Sol. 34 (1969) 569.
[3] T.S. Nikolov, M. Aroyo, E. Klein, K. Ikonopisov, Thin Solid Films 30 (1975) 37.
[4] V. Dolocan, F. Iova, Phys. Stat. Sol. A 64 (1981) 755.
[5] L. Leontie, M. Caraman, G.I. Rusu, J. Optoelectron. Adv. Mater. 2/4 (2000) 385.
[6] L. Leontie, M. Caraman, M. Alexe, C. Harnagea, Surf. Sci. 480 (2002) 507.
[7] T.A. Raju, A.A. Talwai, J. Appl. Phys. 52 (1981) 4877.
[8] E.Y. Wang, K.A. Pandelisev, J. Appl. Phys. 52 (1981) 4818.
[9] H.A. Harwig, Z. Anorg. Allg. Chem. 444 (1978) 151.
[10] H.A. Harwig, A.G. Gerards, Thermochim. Acta 28 (1979) 121.
[11] K.Z. Fung, A.V. Virkar, J. Am. Ceram. Soc. 74 (1991) 1970.
[12] K.Z. Fung, J. Chen, A.V. Vikar, J. Am. Ceram. Soc. 76 (1993) 2405.
[13] L.G. Sillen, Ark. Kemi Mineral. Geol. 12A (1937) 1.
[14] G. Gattow, H.Z. Schröder, Anorg. Allg. Chem. 318 (1962) 176.
[15] G. Gattow, D.Z. Schütze, Anorg. Allg. Chem. 328 (1964) 44.
[16] A.V. Joshi, N. Weber, J. Mater. Sci. 25 (1990) 1237.
[17] A.A. Agasiev, Y.Y. Guseinov, Mater. Res. Bull. 21 (1986) 765.

[18] L. Leontie, M. Caraman, M. Delibas, G.I. Rusu, Mater. Res. Bull. 36/9 (2001) 1629.
[19] J. George, K.S. Joseph, Thin Solid Films 148 (1987) 181.
[20] R.H. Misho, W.A. Murad, Z.A.R. Salmin, Solar Energy Mater. 21 (1991) 347.
[21] G. Bandoli, D. Barreca, E. Brescacin, G.A. Rizzi, E. Tondello, Chem Vap. Depos. 2 (1996) 238.
[22] M. Alexe, J.F. Scott, C. Curran, N.D. Zakharov, D. Hesse, A. Pignolet, Appl. Phys. Lett. 73 (1998) 1592.
[23] J.A. Switzer, Science 284 (1999) 293.
[24] E.W. Bohannan, J.A. Switzer, Solid State Ionics 131 (2000) 97.
[25] T. Takeyama, N. Takahashi, T. Nakamura, S. Ito, J. Phys. Chem. Solids 65 (2004) 1349.
[26] C.G. Jin, X.G. Li, J. Mater. Chem. 13 (2003) 1743.
[27] Liang Li, Lide Zhang, Mater. Lett. 59 (2005) 1223.
[28] C.C. Huang, K. Z. Fung, Electrochem. Solid State Lett., 8 (2005) 204.
[29] H. Over, A.P. Seitsonen, Science 297 (2002) 2003.
[30] C.C. Huang, K.Z. Fung, Mat. Res. Bul. 41 (2006) 110.